3D Myocardial T_1 Mapping Using Saturation Recovery

Giovanna Nordio, MRes,[1]* Markus Henningsson, PhD,[1] Amedeo Chiribiri MD,[1] Adriana D.M. Villa, MD, PhD,[1] Torben Schneider, PhD,[2] and René M. Botnar, PhD[1,3,4,5,6]

Purpose: To propose a 3D quantitative high-resolution T_1 mapping technique, called 3D SASHA (saturation-recovery single-shot acquisition), which combines a saturation recovery pulse with 1D-navigator-based-respiratory motion compensation to acquire the whole volume of the heart in free breathing. The sequence was tested and validated both in a T_1 phantom and in healthy subjects.

Materials and Methods: The 3D SASHA method was implemented on a 1.5T scanner. A diaphragmatic navigator was used to allow free-breathing acquisition and the images were acquired with a resolution of $1.4 \times 1.4 \times 8\,mm^3$. For assessment of accuracy and precision the sequence was compared with the reference gold-standard inversion-recovery spin echo (IRSE) pulse sequence in a T_1 phantom, while for the in vivo studies (10 healthy volunteers) 3D SASHA was compared with the clinically used 2D MOLLI (3-3-5) and 2D SASHA protocols.

Results: There was good agreement between the T_1 values measured in a T_1 phantom with 3D SASHA and the reference IRSE pulse sequences (1111.6 ± 31 msec vs. 1123.6 ± 8 msec, $P = 0.9947$). Mean and standard deviation of the myocardial T_1 values in healthy subjects measured with 2D MOLLI, 2D SASHA, and 3D SASHA sequences were 881 ± 40 msec, 1181.3 ± 32 msec, and 1153.6 ± 28 msec respectively.

Conclusion: The proposed 3D SASHA sequence allows for high-resolution free-breathing whole-heart T_1-mapping with T_1 values in good agreement with the 2D SASHA and improved precision.

Level of Evidence: 2

J. MAGN. RESON. IMAGING 2017;00:000–000

Myocardial fibrosis is a common manifestation for several cardiomyopathies and it is one of the main predictors of future cardiac outcome.[1] Quantitative T_1 mapping is a noninvasive tissue characterization technique that allows to differentiate between healthy and diseased tissues, based on the different environment of their water molecules.[2] In recent years myocardial T_1 mapping techniques have been widely used to visualize both local and diffuse fibrosis.[3,4] T_1-mapping compares favorably to the late gadolinium enhancement (LGE) technique both in terms of quantification/staging of disease and fibrosis detection, as LGE can only detect the presence of focal fibrosis in the heart.[2] T_1 mapping sequences acquire multiple images with variable T_1 weighting and uses pixel-wise fitting of the imaging data to an exponential signal recovery model of the longitudinal relaxation to generate a T_1 map. T_1 mapping is often performed before and after the administration of a contrast agent to quantify the extracellular volume fraction.[5] Different techniques have been proposed for T_1 mapping using either inversion-recovery,[6] saturation-recovery,[7] or a combination of the two.[8] The modified Look–Locker inversion-recovery (MOLLI) technique uses a 180° pulse to invert the longitudinal magnetization and a number of single-shot images are acquired during the mid-diastolic rest period at different inversion times.[6] A number of "pause" cardiac cycles are typically performed, in which no images are acquired, to allow the longitudinal magnetization to fully recover between successive inversion pulses. This technique provides precise T_1 maps

View this article online at wileyonlinelibrary.com. DOI: 10.1002/jmri.25575

Received Aug 23, 2016, Accepted for publication Nov 18, 2016.

*Address reprint requests to: G.N., Biomedical Engineering Department, King's College London, Imaging Sciences Division, 4th floor, Lambeth Wing, St Thomas' Hospital, London SE1 7EH, UK. E-mail: giovanna.nordio@kcl.ac.uk

From the [1]Division of Imaging Science and Biomedical Engineering, King's College London, London, UK; [2]Philips Health Systems, London, UK; [3]Wellcome Trust and EPSRC Medical Engineering Center, King's College London, UK; [4]BHF Centre of Excellence, King's College London, UK; [5]NIHR Biomedical Research Centre, King's College London; and [6]Pontificia Universidad Católica de Chile, Escuela de Ingeniería, Santiago, Chile

SUPPLEMENTARY MATERIAL is linked to the online version of the article at http://www.wileyonlinelibrary.com.cpt

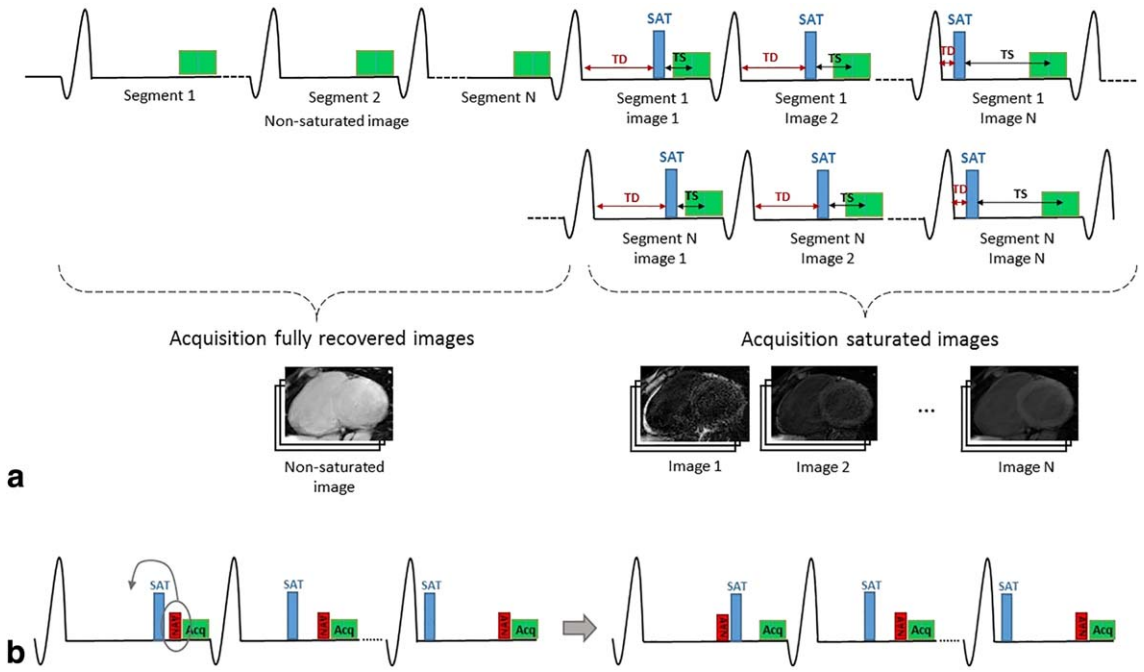

FIGURE 1: a: Schematic diagram of the 3D SASHA pulse sequence. First, the images without any magnetization preparation are acquired, then an interleaved acquisition is used for the saturated images, where the saturation times (TS) and the delay time (TD) is varied. b: For the shortest TS the position between the saturation pulse (SAT) and the navigator (NAV) is swapped.

with high reproducibility; however, the quantification accuracy is affected by the perturbation of the longitudinal signal recovery due to the repeated image acquisitions, causing a general underestimation of myocardial T_1.[9] The MOLLI technique is highly dependent on heart rate and this can severely affect the accuracy, as higher heart rates may not allow the longitudinal magnetization to fully recover to the initial state. A different solution has been proposed, which uses a saturation-recovery pulse, called the saturation-recovery single-shot acquisition (SASHA) imaging sequence.[7] With this technique, one single-shot image is acquired after the application of a saturation pulse, typically in mid-diastole. This is repeated in subsequent heartbeats with varying time delays after the saturation pulse, thereby providing images with varying T_1 weighting. Thanks to the use of a saturation pulse, which removes any spin history, the SASHA sequence is less susceptible to T_1 errors caused by heart rate variations[10] and there is no requirement for pause cycles between image acquisition, making the scan efficiency higher compared to MOLLI. However, there is a loss in precision due to the smaller dynamic range of the measured longitudinal magnetization.

Existing MOLLI and SASHA techniques are limited in spatial resolution and coverage due to the need for breath-holding, which is required to minimize respiratory motion artifacts. Typically, only a single low-resolution 2D slice can be acquired for each breathhold with both MOLLI and SASHA. Due to the increased scan time associated with higher-resolution 3D image acquisition of the heart, free-breathing imaging is necessary and respiratory motion compensation imperative to ensure diagnostic image quality. Some techniques for 3D T_1 mapping have already been proposed.[11–13] However, these are based on an inversion recovery acquisition and consequently they are heart rate-dependent. Instead, the SASHA sequence appears to be a promising candidate for volumetric free-breathing T_1 mapping of the whole heart, due to its high scan efficiency and quantification accuracy, and its robustness to heart-rate variations which may occur over the course of a 5–10-minute scan.

In this work, we sought to develop and assess a multi-shot high-resolution 3D SASHA sequence with improved spatial resolution and coverage that can be acquired in free-breathing with respiratory motion compensation.

Materials and Methods

Pulse Sequence Scheme

All data were acquired on a 1.5T Ingenia MR system (Philips, Best, The Netherlands). The proposed 3D SASHA pulse sequence enables the acquisition of whole-heart T_1 mapping in free breathing. To this end, the 2D SASHA sequence[7] was modified to make the sequence compatible with a 3D segmented *k*-space acquisition. The sampling scheme used for 3D SASHA is shown in Fig. 1a. First, all image *k*-space segments with no magnetization preparation were acquired, which we term "infinity image" (as we assume it is acquired after an infinite saturation delay time during data fitting). This was followed by the interleaved segmented acquisition with preceding saturation pulse and increasing saturation delays. To ensure all *k*-space segments of the infinity image were acquired at equilibrium magnetization, "pause" cardiac cycles were added between the acquisitions of these segments. During these pauses,

all RF pulses and data acquisition were switched off to allow for full T_1 recovery.

To compensate for respiratory motion a 1D hemidiaphragmatic navigator (NAV) was used. Typically, the navigator is performed immediately before the image acquisition to allow prospective motion correction and ensure high temporal correlation between NAV and image acquisition. However, for the shortest saturation time the navigator signal may be insufficient for reliable motion estimation. Therefore, the position between the saturation pulse and the navigator was swapped for the shortest saturation time (40 msec) (Fig. 1b).

To minimize the sensitivity to B_1 inhomogeneities the saturation pulse used for imaging was a composite saturation pulse with a train of four rectangular pulses with numerically optimized flip angles (respectively 72°, 92°, 126°, 193°), each followed by a dephasing gradient.[14] Imaging was performed with a 32-channel cardiac coil and the heart rate was monitored using the vector electrocardiogram (VCG) for the whole duration of the scan.

Data acquisition was performed with a segmented 3D steady-state free-precession (SSFP) technique and imaging parameters included: field of view (FOV) = 300 × 300 × 90 mm^3, repetition time / echo time (TR/TE) = 3.2/1.6 msec, image resolution = 1.4 × 1.4 mm^2, slice thickness = 8 mm, flip angle (FA) = 35°, parallel imaging with SENSE factor of 2 in phase-encoding direction, 10 start-up echoes, Cartesian acquisition with radial *k*-space shutters, slice-selective RF pulse. Thirty segments of the *k*-space were acquired per heartbeat with a low-high *k*-space ordering and an acquisition window duration of 90 msec.

Simulations

The proposed segmented multishot SASHA pulse sequence was simulated using the Bloch equations in MatLab R2014a (MathWorks, Natick, MA). The simulations were performed to analyze the effect of the added "pause" cardiac cycles between acquisitions of the infinity images and to investigate the optimal number of pauses for a given heart rate to ensure complete longitudinal magnetization recovery. The simulations for an SSFP sequence were performed for heart-rates between 60–100 bpm, T_1 of 1100 msec (precontrast myocardial T_1 at 1.5T), T_2 of 45 msec, 40 RF excitations per segment, FA of 35°, TR of 2.8 msec, and for different numbers of "pause" cardiac cycles.

Phantom Experiments

A phantom with nine agar/$NiCl_2$ vials was used for imaging, with T_1 values ranging from 250 msec to 1500 msec,[15] to compare T_1 measurements between the gold standard inversion-recovery spin echo (IRSE) technique, 2D MOLLI, 2D SASHA, and the proposed 3D SASHA. The IRSE pulse sequence was performed with 10 inversion times varying from 100–2000 msec. The reference T_1 measurements were compared to 2D MOLLI, 2D SASHA, and the proposed 3D SASHA, in order to validate the imaging technique. Sequence parameters for the spin echo sequence were: FOV = 200 × 200 mm^2, image resolution = 3.1 × 3.1 mm^2, 10 mm slice thickness, TR = 8000 msec, and TE = 5.9 msec.

The MOLLI sequence was acquired with the following parameters: FOV = 300 × 280 mm, TR/TE = 2.6/1.3, image resolution = 1.7 × 2.1 mm, slice thickness = 10 mm, FA = 35°, scan time of about 12 seconds. The acquisition parameters for the 2D SASHA sequence were: FOV = 300 × 280 mm^2, TR/TE = 2.6/1.3, image resolution = 1.7 × 2.1 mm^2, slice thickness = 10 mm, FA = 70°, 100–700 msec saturation time (TS) for a heart rate of 60 bpm, parallel imaging with SENSE factor of 2 in the phase-encoding direction. For the 3D SASHA sequence the saturation times (TS) were 100–700 msec for a heart rate of 60 bpm. All three imaging techniques were reconstructed to the same in-plane resolution of 1.25 × 1.25 mm^2.

The proposed 3D SASHA sequence was acquired with fewer T_1-weighted images along the Mz recovery curve compared to the conventional 2D SASHA sequence (9 instead of 11, including the "infinity" image) in order to keep the total scan time within 5 minutes.

All sequences were triggered with a simulated heart rate of 60 bpm and signal reception was performed with a 32-channel cardiac coil

To validate the findings of the simulations and evaluate the optimal flip angle and number of "pause" heart cycles added between acquisitions of the fully recovered "infinity" images, the phantom was imaged using the 3D SASHA sequence with a different number of pauses and by changing the FA within the range from 25° to 85° with 10° increments. This experiment was repeated for 3D SASHA with 0, 1, 2, and 3 pause cycles for the infinity image.

In Vivo Studies

The study was performed in accordance with the Declaration of Helsinki (2000). All subjects involved in this study provided written informed consent with study approval from the Institutional Review Board (15/NS/0030). Ten healthy volunteers without a history of heart disease were imaged using 2D MOLLI, 2D SASHA, and 3D SASHA sequences. The same imaging parameters used for the phantom experiment were employed for the in vivo study. The acquisition of the 3D SASHA sequence was performed in free-breathing with a nominal scan duration of 4:14 (min:sec) for a heart rate of 60 bpm and 100% scan efficiency. A 1D diaphragmatic navigator was used for respiratory motion compensation with a gating window of 5 mm and a tracking factor of 0.6.

Following the validation with Bloch simulations and phantom studies, three "pause" cardiac cycles were used for all in vivo imaging.

Image Analysis

The T_1 maps were reconstructed offline using MatLab. The T_1 values were calculated by fitting the image signal intensities to a three-parameter exponential recovery curve using the fitting procedure proposed by Barral et al.[16] Regions of interest (ROIs) were manually drawn on the phantom images and in the myocardium and the measured average T_1 values were expressed as mean ± standard deviation.

Accuracy and precision are the two criterions used to evaluate the efficiency of quantitative T_1 mapping.[17] For the phantom experiments the accuracy of the 3D SASHA T_1 maps was evaluated by comparing the mean T_1 values with the reference measurements from the IRSE experiment using a Kruskal–Wallis test. A Bland–Altman analysis was performed to compare the different techniques

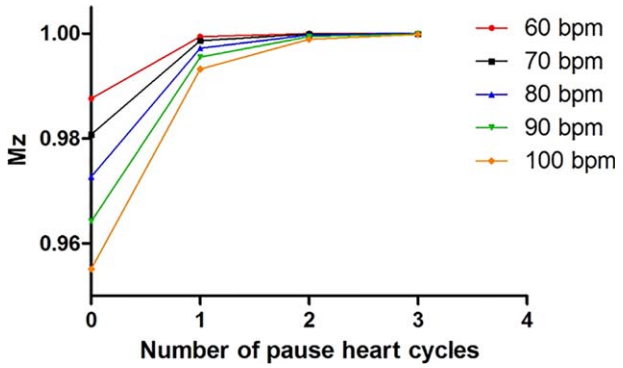

FIGURE 2: The graph shows the recovered longitudinal magnetization Mz (y-axis) as a function of different number of "pause" cardiac cycles (x-axis) between the acquisitions of the images without any magnetization preparation, for different heart rates.

and to evaluate the agreement between them. For in vivo studies the myocardial T_1 values were compared with the values measured with the 2D SASHA and 2D MOLLI sequences.

The standard deviation of the T_1 measurements was used to quantify the precision, ie, the spatial variability of T1 across the selected ROI, of each imaging technique.[10]

Sharpness of the myocardial borders was used as a criterion to quantify the performance of motion correction and was measured using dedicated software. The sharpness was calculated as a percentage of the steepness of the edges of the myocardium, where 100% corresponds to an ideal step edge.[18] Measurements were done on the myocardial septum for both the 2D SASHA and the 3D SASHA T_1 maps. Two blinded expert reviewers (Reviewer 1 with more than 10 years and Reviewer 2 with 5 years of experience in cardiovascular MRI) scored the T_1 maps of all volunteers based on image quality, which includes both myocardial sharpness and signal homogeneity. The scale for scoring the image quality was: 1 poor, 2 average, 2 good, 3 very good, and 5 excellent image quality. The Wilcoxon rank *t*-test was used to evaluate the statistical difference between 2D SASHA and 3D SASHA. The median was calculated and presented together with the 75% and 25% of the median itself.[19]

The American Heart Association (AHA) 17-segment[20] models for the 2D SASHA and 3D SASHA techniques were used to compare the two techniques and to provide a 3D visualization of the left ventricle. The myocardial T_1 values of the whole volume were measured for 16 AHA segments (excluding the apical segment 17, not included in short axis view as per clinical standard) in three slices (apex, mid, base). Each segment of the final model was calculated as the average of the same segment between all the volunteers.

For statistical analysis, GraphPad Prism v. 5 for Windows (GraphPad Software, La Jolla, CA) was used and $P < 0.05$ was used to define the statistical significance.

Results

Simulations

Figure 2 shows the steady-state M_z magnetization for a tissue with T_1 similar to healthy myocardium on 1.5T ($T_1 = 1100$ msec) during the acquisition of the infinity image as a function of different numbers of "pause" cardiac cycles (from zero to three). The recovery of M_z depends both on the number of pauses added between the infinity images and on the heart rate. M_z returns to the equilibrium magnetization after two pause cardiac cycles for heart rates lower or equal than 60 bpm. However, three pauses are more robust for higher heart rates, and may ensure full recovery of M_z even in the presence of heart-rate variability, which can occur during a 5–10-minute scan. Thus three pauses were chosen for all in vivo studies.

Phantom Experiments

Table 1 summarizes the mean values and standard deviations calculated with IRSE, 2D MOLLI, 2D SASHA, and 3D SASHA sequences. An ROI was selected for each of the nine vials of the phantom and the average T_1 value calculated. The 3D SASHA T_1 map appears more homogeneous and less noisy compared to the 2D SASHA T_1 map (Fig.

TABLE 1. Mean and Standard Deviation for All the Phantom Vials, Respectively for Spin-Echo, 2D MOLLI, 2D SASHA, and 3D SASHA Sequences

Phantom vial	Reference T1 [msec]	Spin-echo T1 [msec]	2D MOLLI T1 [msec]	2D SASHA T1 [msec]	3D SASHA T1 [msec]
1	430	431.8 ± 10	391 ± 2	434.9 ± 7	442.4 ± 4
2 (Myocardial-like)	1090	1111.6 ± 31	898.4 ± 5	1104 ± 14	1091.5 ± 9
3	458	459.4 ± 9	451.8 ± 3	462.4 ± 6	471.2 ± 5
4	562	569.3 ± 13	503.5 ± 6	571.1 ± 11	566.2 ± 6
5	1333	1379.7 ± 55	1063.5 ± 8	1374.3 ± 26	1362.6 ± 13
6 (Blood-like)	1489	1559.8 ± 62	1338 ± 8	1519.1 ± 26	1506.4 ± 19
7	300	301 ± 7	277.3 ± 3	305.2 ± 8	310.7 ± 3
8	803	811.6 ± 17	692.2 ± 4	815.1 ± 13	799.1 ± 5
9	255	253.9 ± 6	252.4 ± 2	260.7 ± 4	268.8 ± 4

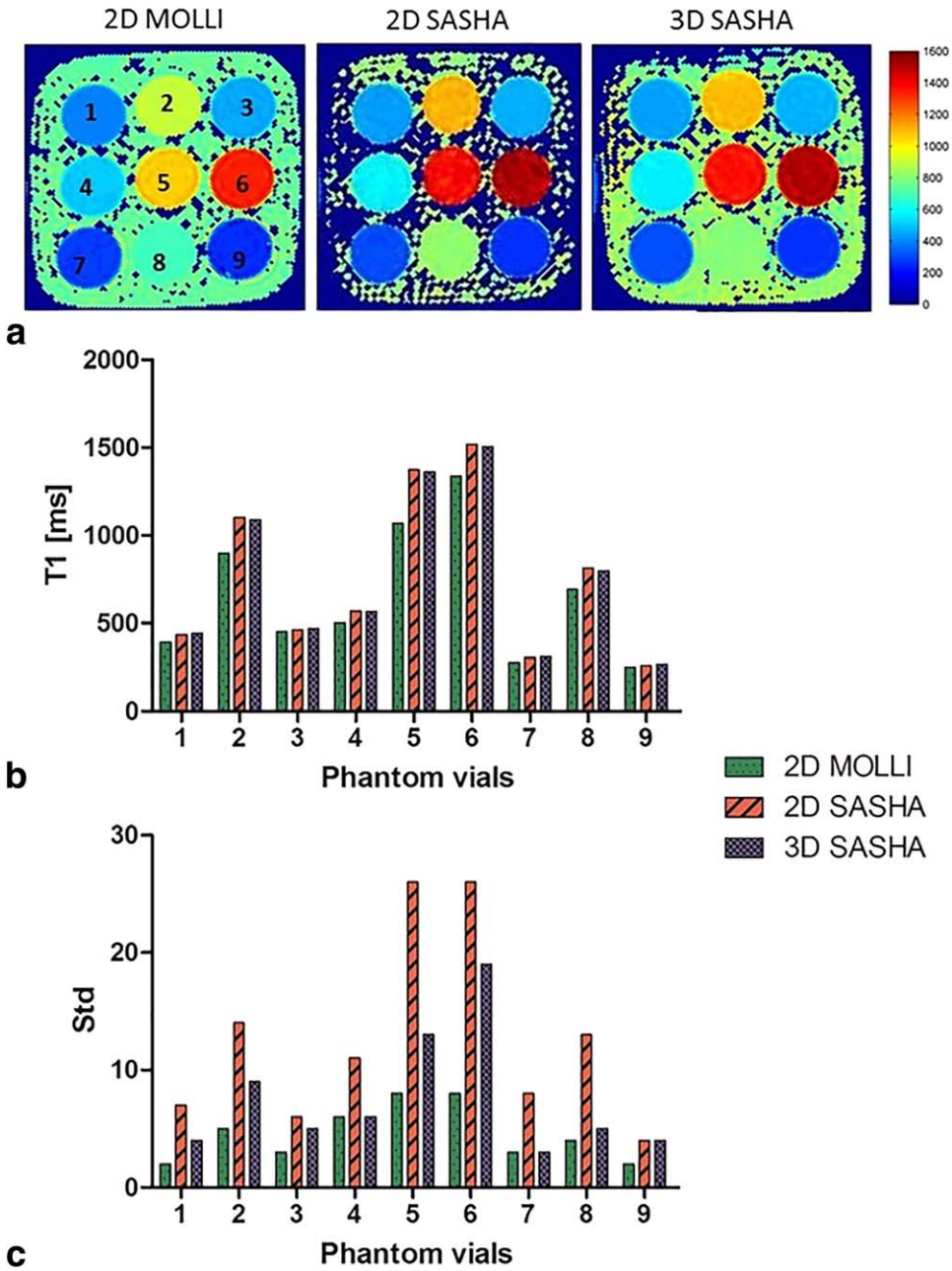

FIGURE 3: a: T_1 map of the phantom obtained using the 2D MOLLI, 2D SASHA, and 3D SASHA sequences. b,c: Mean and standard deviation of the measured T_1 values for all the nine vials.

3a). 3D SASHA and 2D SASHA were found to have similar accuracy, while 2D MOLLI generally underestimates the T_1 values. Although fewer T_1-weighted images were used for the 3D SASHA compared to 2D SASHA (9 for 3D SASHA vs. 11 for 2D SASHA) the precision of the 3D SASHA is higher, as measured by the lower standard deviation (Fig. 3b-c). The Bland–Altman analysis in Fig. 4a compares the reference T_1 values measured with the IRSE sequence with the T_1 values measured respectively with 3D SASHA and 2D SASHA sequences. For the 3D SASHA, the mean difference is 6.6 msec and the limits of 95% agreement are –36.6msec and 49.8 msec, while for the 2D SASHA the mean difference is 3.5 msec and the limits of 95% agreement are –25.3 msec and 32.3 msec. The 3D SASHA T_1 values are in good agreement with the 2D SASHA T_1 values with significant correlation ($P < 0.0001$, $r = 0.9998$). The estimated T_1 values using the 3D SASHA and the 2D SASHA sequences correlate extremely well ($r = 0.9997$) with the IRSE sequence (Fig. 4b,c). The agreement in T_1 values between the 3D SASHA and IRSE was confirmed by the Kruskal–Wallis test ($P = 0.9947$). The T_1 estimation for the vial with the highest T_1 value deviated from the

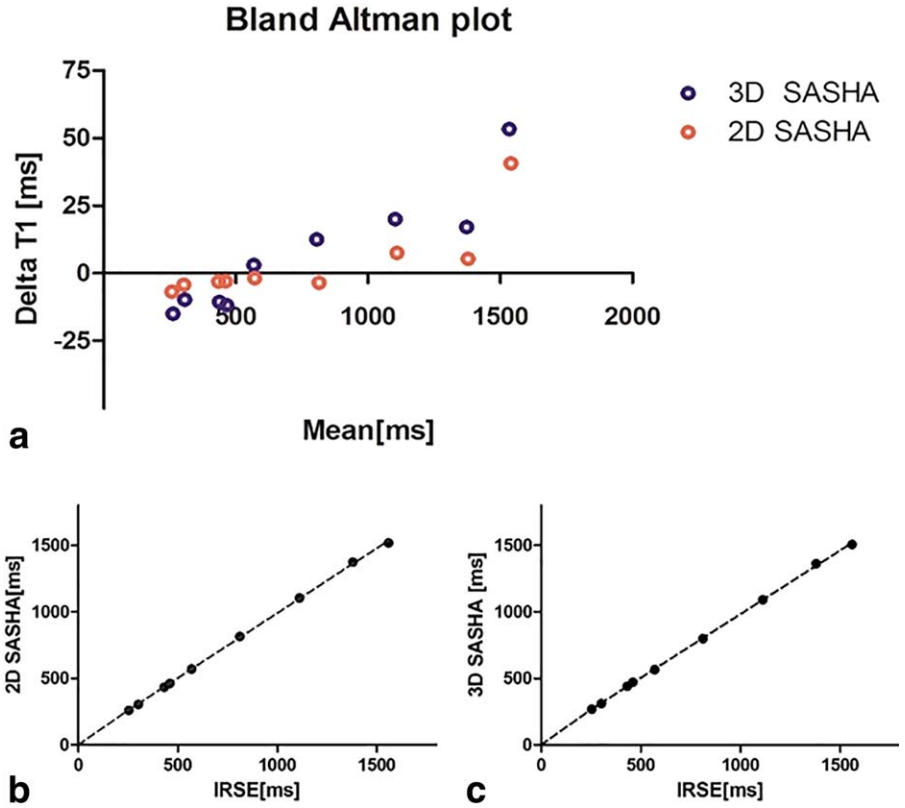

FIGURE 4: a: Bland–Altman analysis between IRSE and 2D SASHA (in red), and 3D SASHA (in blue) sequences. b,c: Agreement between IRSE and 2D SASHA and 3D SASHA sequences.

expected line of identity due to an insufficient recovery time between successive inversion pulses used for the IRSE sequence. This led to a wrong estimation of the highest T_1 values with the IRSE sequence and consequently to a mismatch between the 3D SASHA and the IRSE T_1 value for the vial with the highest T_1.

Figure 5 shows the results obtained from the phantom experiment using different combinations of FAs and number of "pause" heart cycles; only the results from the vial with myocardial-like T_1 are illustrated. The graph shows the difference between the reference T_1 value and the measured T_1 values, and the best agreement was obtained using an FA of 35° and three "pause" heart cycles, which confirms the results obtained from the simulations.

In Vivo Studies

Figure 6a shows the myocardial T_1 maps of three volunteers obtained with the 2D MOLLI, 2D SASHA, and 3D SASHA sequences. The single T_1-weighted images acquired for Volunteer 2 are shown in Fig. 6b. For all volunteers there was good agreement between the myocardial T_1 values measured with the 2D SASHA and the 3D SASHA sequences, while the T_1 values obtained with the 2D MOLLI sequence were considerably lower (Fig. 7a). A trend of improvement in terms of precision was visible with the proposed imaging technique compared with the 2D SASHA (Fig. 7b). The average T_1 values of all subjects for the 2D MOLLI, 2D SASHA, and 3D SASHA sequences were 881 ± 32 msec, 1181.2 ± 32msec, and 1153.6 ± 28 msec, respectively. The duration of the 3D SASHA scan was of $12{:}1 \pm 1{:}3$ (min:sec) with a scan efficiency of 32%.

The average myocardial border sharpness measured on the 2D SASHA T_1 maps was significantly higher compared to 3D SASHA T_1 maps (respectively $26\% \pm 2$ and $18\% \pm 3$).

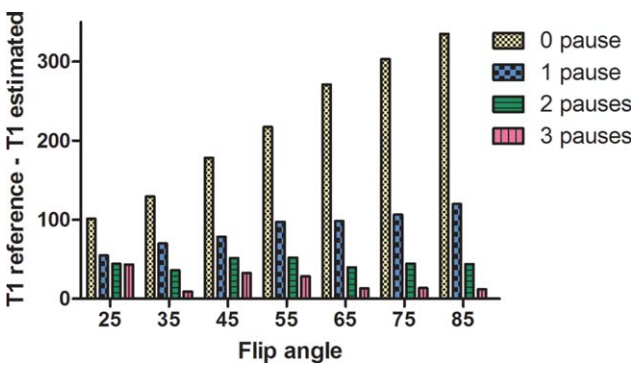

FIGURE 5: The graph shows the difference between the gold standard T_1 and the measured T_1 for vial number 2 (reference $T_1 = 1090$ msec), using different combinations of number of pauses between the acquisition of the "infinity" images (from 0 to 3) and flip angles (from 25° to 85°).

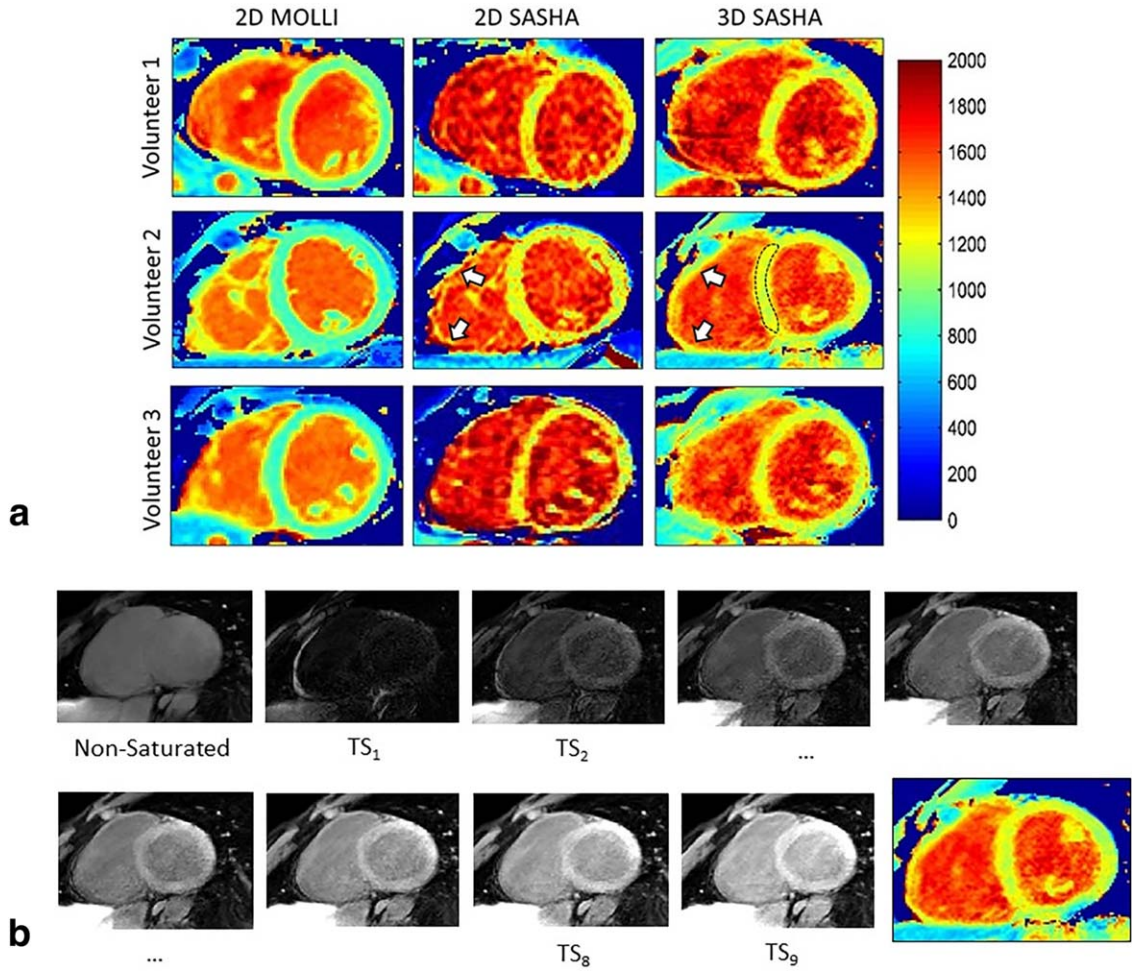

FIGURE 6: a: Mid-ventricular myocardial T_1 maps of three healthy subjects using the sequences 2D MOLLI, 2D SASHA, and 3D SASHA sequences. The average T_1 values were calculated by manually drawing an ROI in the septum of the myocardium. The higher resolution of the 3D SASHA technique allows to better delineate the right ventricle (white arrows). b: Nine images acquired at different saturation times for Volunteer 2.

The agreement in image quality between the observers was 80% for the 2D MOLLI T_1 maps, and 50% for the 2D SASHA and 3D SASHA T_1 maps. In general, we observed better image quality for the 2D MOLLI T_1 maps (median 5, 75% of the median of 5, 25% of the median of 4), with significant statistical difference with both 2D and 3D SASHA (respectively $P = 0.0053$ and $P = 0.0047$). There was no statistical difference between 2D SASHA (median 2, 75% of the median = 3, 25% of the median = 2) and 3D SASHA (median 3, 75% of the median = 3, 25% of the median = 2).

Figure 8 shows the bull's eye plots of the left ventricle for the 2D SASHA and 3D SASHA imaging sequences. The AHA model was calculated for both the mean and standard deviation of the T_1 values measured across the left ventricle. The average myocardial T_1 values are homogeneous across the left ventricle for both of the imaging techniques. The standard deviation for the 3D SASHA is lower compared to the 2D SASHA, which could be explained by the theoretical higher signal-to-noise ratio (SNR) for the 3D technique. However, a higher standard deviation was observed in the inferior wall of the basal slice, which could be explained by slice profile imperfection and motion artifacts.

Discussion

In this study we proposed and validated a free-breathing 3D SASHA sequence for T_1 mapping of the whole left ventricle. The sequence was validated with simulations, phantom, and in vivo experiments.

The proposed 3D T_1 mapping approach was based on the well-established 2D SASHA pulse sequence design.[7] The main difference between 2D SASHA and the proposed 3D sequence was that segmented *k*-space acquisition was required to enable high-resolution 3D acquisition. A Cartesian acquisition with radial *k*-space shutter was used, which is commonly used for magnetization-prepared heart imaging. However, no further analysis was conducted to investigate the effect of the acquisition scheme.

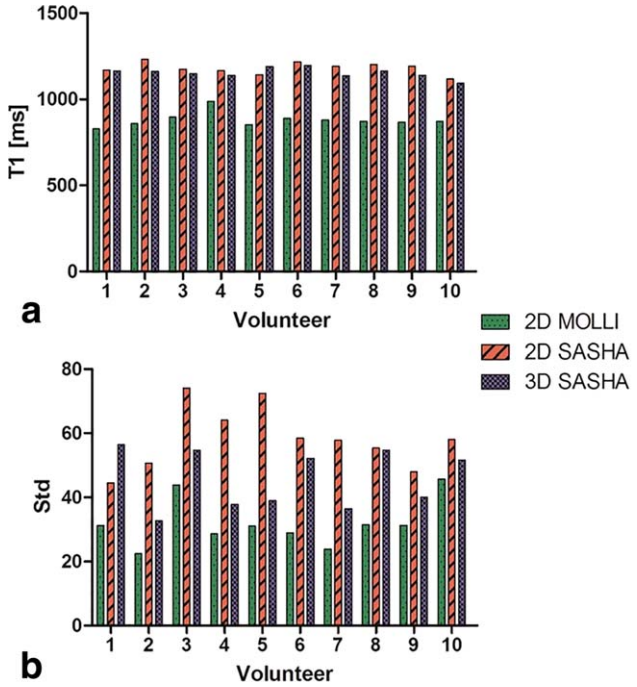

FIGURE 7: Mean and standard deviation of the myocardial T_1 measurements of the 10 healthy subjects using 2D MOLLI, 2D SASHA, and 3D SASHA sequences.

The in vivo studies confirmed the phantom measurements in terms of accuracy between 2D SASHA and 3D SASHA sequences, as similar average myocardial T_1 values were obtained. The standard deviations of the 3D T_1 measurements were lower compared to the 2D SASHA. Improved subjective image quality with 3D SASHA over 2D SASHA was observed, although this finding was not significant. This could be attributed to the fact that a 3D imaging sequence inherently benefits from higher SNR compared to a 2D method.

As demonstrated in the phantom experiments, the proposed 3D T_1 mapping imaging sequence improves accuracy compared to 2D MOLLI and precision compared to 2D SASHA. This is a promising result and warrants further evaluation of the 3D SASHA imaging technique in clinical practice. Also, a free-breathing T_1 mapping approach would be useful in patients who cannot hold their breath due to respiratory problems.

Other 3D T_1 mapping techniques have already been proposed,[11–13] which use an inversion recovery pulse to generate T_1 weighting. The proposed 3D SASHA technique uses a saturation recovery pulse, which has the advantage of completely erasing the history of the longitudinal magnetization between the acquisitions, thus reducing the heart rate dependency as well as improving scan efficiency. Further work will investigate other available T_1 mapping techniques with the proposed 3D SASHA sequence. For the 3D SASHA imaging techniques, an incomplete and incorrect saturation could be an important source of errors in the final T_1 map. In the proposed 3D SASHA sequence a

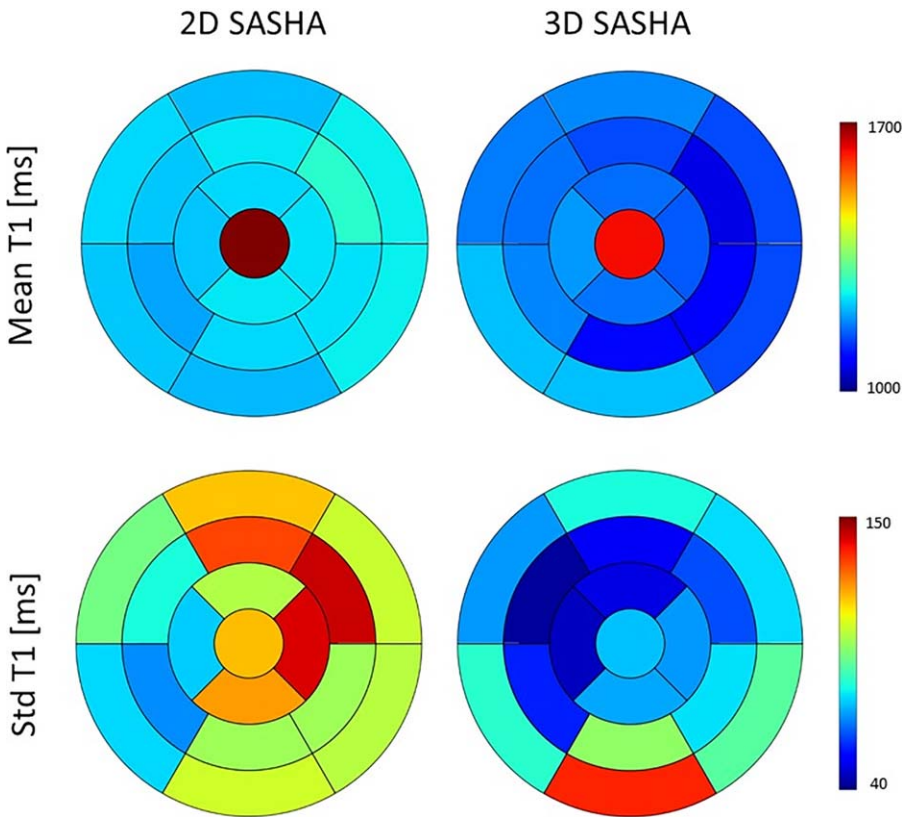

FIGURE 8: Bull's eye plots of the left ventricle. Mean T_1 values (top row) and standard deviations of the T_1 measured (bottom row) are shown for both 2D SASHA and 3D SASHA sequences. Each segment is the average between 10 volunteers and contains the average myocardial T_1. The red central segment represents the blood.

composite saturation pulse was used, with a saturation efficiency of 0.989 ± 0.005, estimated from the exponential fitting curve.[7] The high saturation efficiency confirms the results reported from previous studies.[7] The sharpness of the septum was significantly lower with the 3D SASHA compared to the 2D SASHA T_1 map. This is likely due to residual respiratory motion artifacts. Improved respiratory motion compensation strategies, such as self-navigation[21] or image-based navigation,[22–24] may improve image sharpness while simultaneously helping to reduce scan time. Nevertheless, the visual score test showed a trend of improved image quality for the 3D SASHA compared to the 2D SASHA T_1 maps. In general, better image quality and better visualization of the myocardial borders would be beneficial where trasmurality of scar should be assessed. In addition, high-resolution T_1 mapping may be especially beneficial for fibrosis quantification in the thin wall of the right ventricle. The AHA model showed in general a good homogeneity of the myocardial T_1 values measured across the left ventricle. However, T_1 values in the lateral wall of the mid ventricle were somewhat lower compared to other segments. This is consistent with previous findings showing lower T_1 values in this region, which is likely due to susceptibility artifacts caused by the air–myocardium interface.[25]

In this work a 3-3-5 MOLLI scheme was used, which was the clinically used T_1 mapping technique at the time of the study. Recently, the 5-3 MOLLI scheme has become more popular, due to the shorter breath-hold duration. Further work is required to compare the precision, accuracy, and clinical merits of more recent T_1 mapping techniques with the proposed 3D SASHA.[9]

The proposed 3D SASHA imaging sequence has been extensively tested and validated with simulations, phantom studies, and in vivo experiments on healthy volunteers. Further work is required to evaluate this technique in patients with myocardial scar, as well as for postcontrast T_1 mapping.

Image resolution of the 3D SASHA sequence is mainly limited by the scan time, which is ~12 minutes for the current spatial resolution of $1.4 \times 1.4 \times 8\,\text{mm}^3$. The implementation of novel motion compensation techniques, such as image-based navigation, correcting for both translational and nonrigid motion,[22] removes the requirement for gating and allows using all acquired data for image reconstruction, thereby significantly reducing scan time or increasing spatial resolution. In addition, improved motion compensation may also improve myocardial sharpness and overall image quality. The use of compressed sensing reconstruction could also further accelerate imaging time.[26]

An additional step of retrospective image registration[27] or removal of severely motion corrupted images could be beneficial to correct for residual motion in the T_1 map, which could further improve the reliability of the T_1 measurements.

Scan time is also affected by the number of pauses added between the *k*-space segments of the infinity images. Reduction of the number of pauses could be achieved by introducing some subject-specific correction in the fitting step. A reduced number of images acquired with the 3D SASHA sequence could be another possible solution to shorten the acquisition time, although the trade-off between quantification precision and total acquisition time will have to be investigated further.

In conclusion, the proposed 3D SASHA T_1 mapping technique allows acquiring high-resolution myocardial T_1 maps of the whole left ventricle completely in free breathing with good accuracy. While the accuracy is in the range of the 2D SASHA sequence, the precision is improved.

Acknowledgments

Contract grant sponsor: the EPSRC Centre for Doctoral Training in Medical Imaging; contract grant number: EP/L015226/1; Contract grant sponsor: Philips Healthcare; Contract grant sponsor: Centre of Excellence in Medical Engineering funded by the Wellcome Trust and EPSRC; contract grant number: WT 088641/Z/09/Z; Contract grant sponsor: Department of Health via the National Institute for Health Research (NIHR) comprehensive Biomedical Research Centre award to Guy's & St Thomas' NHS Foundation Trust in partnership with King's College London and King's College Hospital NHS Foundation Trust. The views expressed are those of the authors and not necessarily those of the NHS, the NIHR, or the Department of Health

References

1. Burt JR, Zimmerman SL, Kamel IR, Halushka M, Bluemke DA. Myocardial T1 mapping: techniques and potential applications. Radiographics 2014;34:377–395.
2. Mewton N, Liu CY, Croisille P, Bluemke D, Lima JA. Assessment of myocardial fibrosis with cardiovascular magnetic resonance. J Am Coll Cardiol 2011;57:891–903.
3. Iles L, Pfluger H, Phrommintikul A, et al. Evaluation of diffuse myocardial fibrosis in heart failure with cardiac magnetic resonance contrast-enhanced T1 mapping. J Am Coll Cardiol 2008;52:1574–1580.
4. Flett AS, Hayward MP, Ashworth MT, et al. Equilibrium contrast cardiovascular magnetic resonance for the measurement of diffuse myocardial fibrosis: preliminary validation in humans. Circulation 2010; 122:138–144.
5. Ugander M, Oki AJ, Hsu LY, et al. Extracellular volume imaging by magnetic resonance imaging provides insights into overt and subclinical myocardial pathology. Eur Heart J 2012;33:1268–1278.
6. Messroghli DR, Radjenovic A, Kozerke S, Higgins DM, Sivananthan MU, Ridgway JP. Modified Look-Locker inversion recovery (MOLLI) for high-resolution T1 mapping of the heart. Magn Reson Med 2004;52: 141–146.
7. Chow K, Flewitt JA, Green JD, Pagano JJ, Friedrich MG, Thompson RB. Saturation recovery single-shot acquisition (SASHA) for myocardial T(1) mapping. Magn Reson Med 2014;71:2082–2095.

8. Weingartner S, Akcakaya M, Basha T, et al. Combined saturation/inversion recovery sequences for improved evaluation of scar and diffuse fibrosis in patients with arrhythmia or heart rate variability. Magn Reson Med 2014;71:1024–1034.
9. McDiarmid AK, Broadbent DA, Higgins DM, et al. The effect of changes to MOLLI scheme on T1 mapping and extra cellular volume calculation in healthy volunteers with 3 Tesla cardiovascular magnetic resonance imaging. Quant Imaging Med Surg 2015;5:503–510.
10. Roujol S, Weingartner S, Foppa M, et al. Accuracy, precision, and reproducibility of four T1 mapping sequences: a head-to-head comparison of MOLLI, ShMOLLI, SASHA, and SAPPHIRE. Radiology 2014; 272:683–689.
11. Coniglio A, Di Renzi P, Vilches Freixas G, et al. Multiple 3D inversion recovery imaging for volume T1 mapping of the heart. Magn Reson Med 2013;69:163–170.
12. Clique H, Cheng HL, Marie PY, Felblinger J, Beaumont M. 3D myocardial T1 mapping at 3T using variable flip angle method: pilot study. Magn Reson Med 2014;71:823–829.
13. Weingärtner S, Roujol S, Akcakaya M, Basha T, Nezafat R. Free-breathing multislice native myocardial T1 mapping using the slice-interleaved T1 (STONE) sequence. Magn Reson Med 2015;74:115–124.
14. Ogg RJ, Kingsley PB, Taylor JS. WET, a T1- and B1-insensitive water-suppression method for in vivo localized 1H NMR spectroscopy. J Magn Reson B 1994;104:1–10.
15. Captur G, Gatehouse P, Kellman P, et al. A T1 and ECV phantom for global T1 mapping quality assurance: the T1 mapping and ECV standardisation in CMR (T1MES) program. J Cradiovasc Magn Reson 2016;18:1–3.
16. Barral JK, Gudmundson E, Stikov N, Etezadi-Amoli M, Stoica P, Nishimura DG. A robust methodology for in vivo T1 mapping. Magn Reson Med 2010;64:1057–1067.
17. Kellman P, Hansen MS. T1-mapping in the heart: accuracy and precision. J Cardiovasc Magn Reson 2014;16:2.
18. Etienne A, Botnar RM, Van Muiswinkel AM, Boesiger P, Manning WJ, Stuber M. "Soap-bubble" visualization and quantitative analysis of 3D coronary magnetic resonance angiograms. Magn Reson Med 2002;48: 658–666.
19. McHugh ML., Interrater reliability: the kappa statistic. Biochem Med (Zagreb) 2012;22:276–282.
20. Cerqueira MD, Weissman NJ, Dilsizian V, et al. Standardized myocardial segmentation and nomenclature for tomographic imaging of the heart. A statement for healthcare professionals from the Cardiac Imaging Committee of the Council on Clinical Cardiology of the American Heart Association. Int J Cardiovasc Imaging 2002;18:539–542.
21. Stehning C, Bornert P, Nehrke K, Eggers H, Stuber M. Free-breathing whole-heart coronary MRA with 3D radial SSFP and self-navigated image reconstruction. Magn Reson Med 2005;54:476–480.
22. Henningsson M, Koken P, Stehning C, Razavi R, Prieto C, Botnar RM. Whole-heart coronary MR angiography with 2D self-navigated image reconstruction. Magn Reson Med 2012;67:437–445.
23. Aitken AP, Henningsson M, Botnar RM, Schaeffter T, Prieto C. 100% Efficient three-dimensional coronary MR angiography with two-dimensional beat-to-beat translational and bin-to-bin affine motion correction. Magn Reson Med 2015;74:756–764.
24. Cruz G, Atkinson D, Henningsson M, Botnar RM, Prieto C. Highly efficient nonrigid motion-corrected 3D whole-heart coronary vessel wall imaging. Magn Reson Med 2016 [Epub ahead of print].
25. Rogers T, Dabir D, Mahmoud I, et al. Standardization of T1 measurements with MOLLI in differentiation between health and disease—the ConSept study. J Cardiovasc Magn Reson 2013;15:78.
26. Doneva M, Bornert P, Eggers H, Stehning C, Senegas J, Mertins A. Compressed sensing reconstruction for magnetic resonance parameter mapping. Magn Reson Med 2010;64:1114–1120.
27. Roujol S, Foppa M, Weingartner S, Manning WJ, Nezafat R. Adaptive registration of varying contrast-weighted images for improved tissue characterization (ARCTIC): application to T1 mapping. Magn Reson Med 2015;73:1469–1482.